Toughening Effect of Strain-Induced Crystallites in Natural Rubber

H. P. Zhang,[1] J. Niemczura,[2] G. Dennis,[1] K. Ravi-Chandar,[2] and M. Marder[1]

[1]*Center for Nonlinear Dynamics and Department of Physics, The University of Texas at Austin, Austin, Texas 78712, USA*

[2]*Center for Mechanics of Solids, Structures and Materials and Department of Aerospace Engineering and Engineering Mechanics, The University of Texas at Austin, Austin, Texas 78712, USA*

(Received 22 February 2009; published 18 June 2009)

We study fracture propagation in stretched natural rubber sheets. Experimental results in specimens stretched less than 3.8 times show a monotonic increase in the crack speed with stretch and can be explained by a numerical model based on neo-Hookean theory and Kelvin dissipation. In specimens stretched more than 3.8 times, strain-induced crystallites act as reinforcing and toughening fillers and significantly increase fracture resistance, like nanostructures in other polymeric or biological materials. Consequently, as we increase the amount of stretch, fractures travel slower and slower, and eventually halt altogether.

DOI: 10.1103/PhysRevLett.102.245503 PACS numbers: 62.20.mm, 81.05.Lg, 83.60.Uv, 81.30.−t

Fracture resistance is the property of materials that determines when and how they break. It can be defined as the energy per area required to create a new fracture surface. A very simple view would be that fracture resistance is essentially equal to the surface energy. However, this viewpoint is a severe over-simplification; studies have shown that adding small amounts (~1% in volume fraction) of nanometer-sized fillers, such as rubber particles [1,2] or nanotubes [3], can greatly improve the fracture resistance of a polymeric matrix. Many tough natural materials (usually of biological origin), such as nacre, bone, and spider silk [4,5], also contain nanostructures embedded in an amorphous matrix. Like their man-made counterparts, all these biological materials show greater resistance to fracture than one might expect from the mechanical properties of the component parts.

We have found a similar toughening mechanism in stretched natural rubber containing crystallites induced by stretching. These strain-induced crystallites, coexisting with an amorphous background, are tens of nanometers in size, deform in response to macroscopic loading and act as *in situ* fillers [6–8]. The toughening of rubber by stretching is so severe that it leads to a very counter-intuitive phenomenon. As we stretch rubber by increasing amounts, past a certain stretch ratio fractures travel slower and slower, and eventually halt altogether. We are not aware of another case where one pulls on a solid a little bit and it snaps, but pull twice as hard and it holds together.

Our experiments are conducted with 0.15 mm thick sheets of natural latex rubber. Rectangular specimens are stretched in a tensile testing machine [9]. The stretch ratio is defined as the ratio between the dimensions of original and stretched specimens. In the fracture propagation (x) direction it is constrained to $\lambda_x = 1$ and the stretch ratio λ_y in the perpendicular (y) direction is varied between 1 and 5. Once the desired stretch level is attained, the rubber sheet is sandwiched between a pair of rectangular steel frames. All frames have the same length 66 cm in the x direction and different heights in the y direction ($h = 5.1$, 10.2, and 17.8 cm). This frame maintains a fixed grip boundary condition and simulates an infinite strip geometry.

A 1-mm-long cut along the x direction is inserted into the prestretched sheet with a blade [9,10]. The initial cut can lead to either dynamic fracture propagation or a stationary fracture opening depending on λ_y. In case of propagation, the fracture quickly reaches a steady state; the propagating speed (V_c) is measured photographically. Sequential images with resolutions 384×256 pixels are captured at 48 000 frames/sec. Random dots are marked on the specimen for particle velocity measurements by particle image velocimetry. Photo-elastic measurements are also carried out in white-field mode with two parallel circular polarizers. Though experiments were carried out at different temperatures, we mainly present data collected at 24 °C in this Letter.

We have performed numerical simulations based on neo-Hookean theory [11]. The experimentally determined sound speed (or elastic modulus) [9] is used to calibrate the neo-Hookean model. Retraction experiments [12] are performed to determine the parameter controlling the strength of the Kelvin dissipation. The only free parameter in simulations that we vary to match the experiments determines the maximal stretch beyond which a bond snaps.

Experimentally determined fracture speeds are plotted as a function of stored elastic energy in Fig. 1(a) for three different specimen heights. The elastic energy stored in the specimen is calculated as $E = W(\lambda_y)h/\lambda_y$, where h is the height of the *stretched* specimen and $W(\lambda_y)$ is the neo-Hookean elastic energy density functional with parameters published in [9]. Three distinct regimes can be identified in the results displayed. First, for stored energy levels below about 4.0×10^4 J/m^2 the measured fracture speeds increase nearly linearly with the stored energy; scaling of

 © 2009 The American Physical Society

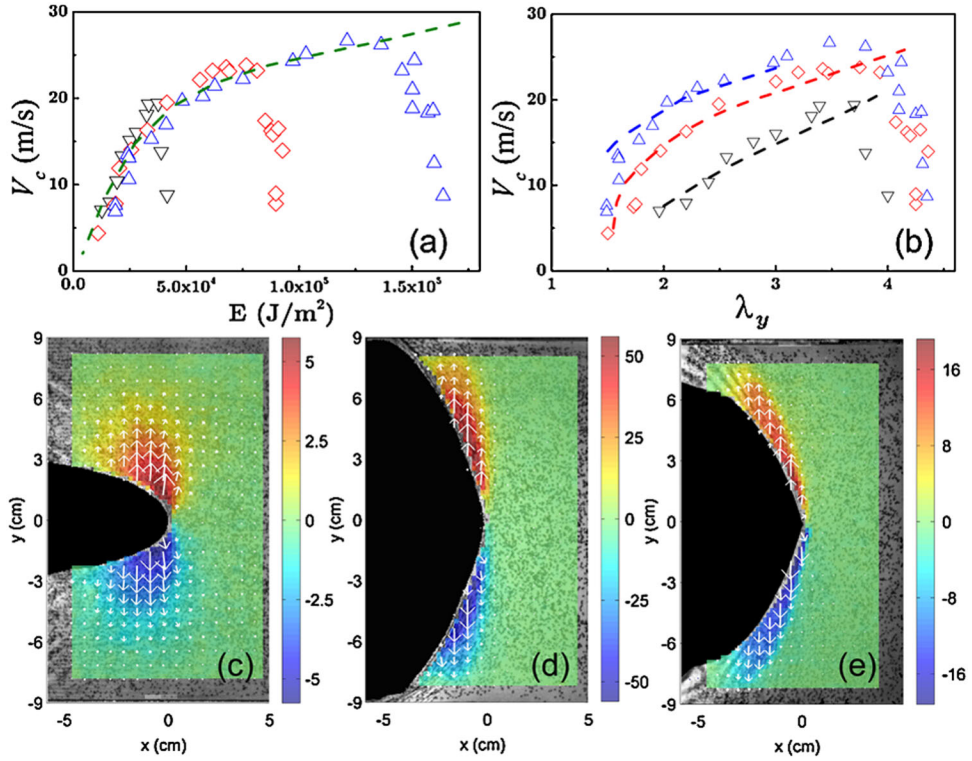

FIG. 1 (color online). Top panels: fracture speed as a function of the stored elastic energy E (a); and of the stretch ratio λ_y (b). In both panels, the symbols correspond to experimental data: △, ◇, and ▽ represent $h = 17.8$, 10.2, and 5.1 cm specimens, respectively. The dashed lines represent results from numerical simulations. Bottom panels: instantaneous particle velocity fields overlayed on images of three steadily propagating fractures in $h = 17.8$ cm specimens: (c) $\lambda_y = 1.5$ and $V_c = 8.3$ m/s; (d) $\lambda_y = 3.1$ and $V_c = 25.6$ m/s; (e) $\lambda_y = 4.35$ and $V_c = 8.7$ m/s. Fractures propagate to the right, and the black regions are the actual opening. Random dots are marked on the rubber for particle velocity measurements. The translucent color layer is coded according to the vertical component of the particle velocity. Color scales are different in each panel. Arrows are velocity vectors. We note that the particle motions in regions very close to the fracture tip are not well resolved in our experiments, especially in the case of $\lambda_y = 3.1$.

this type was reported by Lake *et al.* [10] in a similar parameter regime and is consistent with traditional fracture mechanics analysis of the problem [13]. Second, there is a nonlinear relationship between the stored elastic energy and the fracture speed when the stored energy exceeds 4.0×10^4 J/m^2. The numerical results in these two regimes are shown by the dashed line in Fig. 1(a), which capture the observed fracture behavior quite well. Finally, with further increase in the stored elastic energy, there appears a rapid decrease in the fracture speed ultimately resulting in a stationary crack. The energy level at which this dramatic decrease in fracture speed sets in depends on the specimen height, which means that fracture speed is no longer a single-valued function of available energy and some conventional assumptions of fracture mechanics are breaking down. We explore this further by plotting, in Fig. 1(b), the fracture speed as a function of the initial stretch in the specimen, λ_y; the dashed lines are the numerical results. Up to $\lambda_y = 3.8$ the fracture speed increases monotonically with the stretch and is well predicted by the numerical model; above this level of stretch, the numerical and experimental results depart dramatically. Numerical predictions indicate that the fracture speed should continue to increase with initial stretch. However, experiments show an abrupt decrease in fracture speed, nearly independently of the specimen height. The strong correlation to a critical stretch can be explained in terms of the crystallization of natural latex rubber above a stretch level of about $\lambda_y = 3.8$ as discussed below.

Images of the fracture opening under steady propagation conditions, superimposed with particle velocity vector and contour plots, are shown in Figs. 1(c)–1(e). For $\lambda_y = 1.5$, the fracture speed V_c is much smaller than the shear wave speed (22 m/s) and the crack opening is parabolic in shape as shown in Fig. 1(c). The particle velocity is primarily in the y direction (normal to the crack) and its magnitude is in the range of a few m/s, with significant particle motion ahead of the fracture tip. At a higher stretch of $\lambda_y = 3.1$, the fracture speed V_c is larger than the shear wave speed and the crack opening appears to be wedgelike as shown in Fig. 1(d); particle velocities are significantly higher than the fracture speed and there is very limited motion ahead of the fracture tip. These results on opening shapes and particle velocities are consistent with numerical simulations for $\lambda_y < 3.8$ which implies that viscoelastic dissipation dominates the process in this regime. Beyond

$\lambda_y = 3.8$, experiments show an abrupt decrease in fracture speed. Typical fracture opening and particle velocity field measured in this regime are shown in Fig. 1(e). Although the fracture speed in Fig. 1(e) is almost the same as that in Fig. 1(c), and 40% of that in Fig. 1(d), surprisingly, the fracture opening and the particle velocities bear little resemblance with those in Fig. 1(c), and more with the image shown in Fig. 1(d). The wrinkling of the sheet observed in the crack wake in Fig. 1(e) is also indicative of a possible metric change in the specimen. The marked differences in the fracture opening, kinetic energy distribution and particle velocity are strongly indicative of changes in the fundamental response of the rubber in these different regimes.

For specimens with $\lambda_y > 4.4$ dynamic propagation of the fracture becomes impossible and an initial cut leads to a stationary fracture opening. A photo-elastic picture of such a stationary opening is shown in Fig. 2(a). To obtain this fracture opening, we cut a prestretched ($\lambda_y = 5.45$) specimen with blade along x direction for 1.8 cm. The specimen relaxes into stationary state as shown in the figure without any dynamic propagation. The fracture tips are wedgelike. Away from the crack opening the material is not relaxed, as shown by the nearly uniform color and undeformed orthogonal lines. Material close to the opening is relaxed and shows different colors depending on the amount of relaxation. The interface between relaxed and unrelaxed domains is sharp, which hints at a sudden change of material phases. Similar phase separation between stretched and relaxed materials can also be seen in photo-elastic photos taken from propagating fractures in specimen with $3.8 < \lambda_y < 4.4$, as shown by a pair of bright stripes in Fig. 2(b).

The abrupt decrease in fracture speeds and existence of the stationary opening suggest that fracture resistance in natural rubber increases sharply at $\lambda_y = 3.8$. However, such toughening effect is not observed at high enough temperatures. Systematic measurements at 85 °C show that fracture speed increases monotonically with λ_y up to $\lambda_y = 5$. Furthermore, we find that a stationary fracture obtained at 24 °C can be made to propagate dynamically by heating. The fact that toughening occurs at large stretching and low temperatures suggests that it could be caused by the strain-induced crystallization, which has similar dependence on stretching and temperature [7] and has long been considered responsible for natural rubber's superior toughness observed in low-speed tearing tests [14].

As shown by the x-ray diffraction results in Fig. 3, crystallization starts to occur when $\lambda_y > 3$ at 24 °C. From the width of the diffraction peak, we estimate the crystallites are tens of nanometers in size [6–8]. A broad amorphous halo exists in all specimen, indicating that the majority of the bonds remains amorphous. We expect that the strain-induced crystallites serve the role of nanostruc-

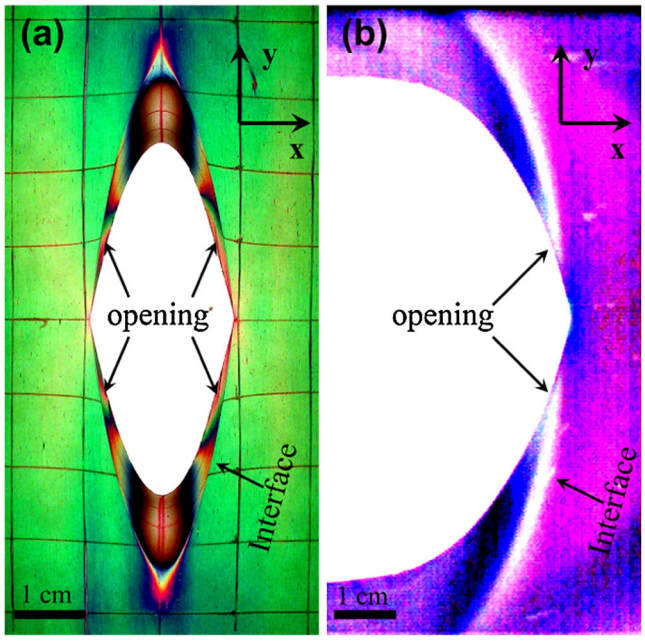

FIG. 2 (color online). Photoelastic picture of a stationary crack (a) and a propagating crack (b). The stretch ratio in (a) is $\lambda_y = 5.45$ and the orthogonal lines, drawn before cutting, are originally separated by 1 cm. In (b), crack propagates at 7.8 m/s and the prestretch is $\lambda_y = 4.25$. A regular fluorescent tube and a flash lamp are used in (a) and (b), respectively, as the light source. Colors in (a) and (b) correspond to local orientation of molecules, which is determined by the stress state. The dark corners in (b) on the right side are artifacts of illumination.

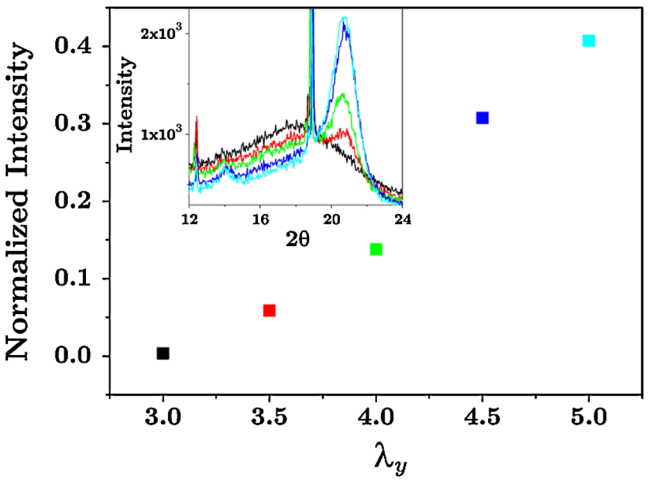

FIG. 3 (color online). Normalized scattering intensity from the crystalline phase, estimated from x-ray diffraction experiments, as a function of stretch ratio λ_y at 24 °C. In the inset, x-ray diffraction data, measured by a Scintag diffractometer with a copper source, are shown for five stretch ratios, which are color coded according to the symbols in main frame. A broad amorphous halo exists in all specimen. The narrow peaks at 12.5° and 18.7° are due to talc mineral fillers in the rubber. A peak emerges at $2\theta = 20.7$ at $\lambda_y = 3$, which is the (210) diffraction peak from the crystallites. We represent the quantity of crystalline phase by the ratio between areas under (210) peak and the amorphous halo, which is plotted in the main frame. Our measurements under pure-shear load ($\lambda_x = 1$) are similar to previous x-ray diffraction studies under uniaxial elongation ($\lambda_x = \lambda_y^{-1/2}$) [6–8].

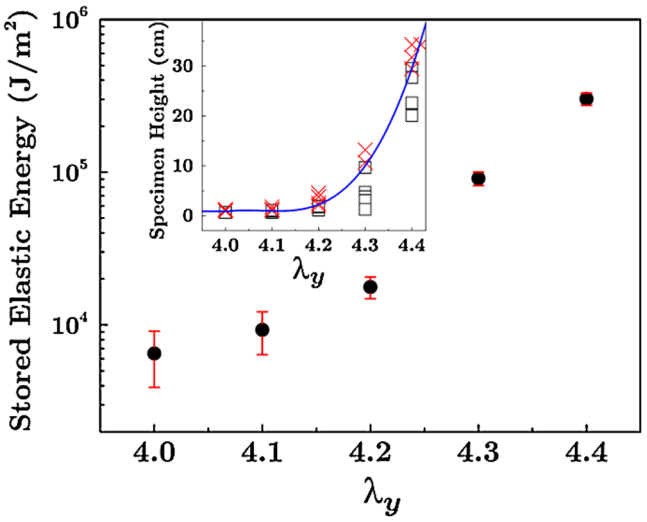

FIG. 4 (color online). Stored elastic energy in specimen of critical height (see text) as a function of stretch ratio λ_y. A phase diagram is shown in the inset, in which the cross $\times$ and square $\square$ correspond to propagating and stationary cracks in response to an initial cut, respectively. The blue line marks the phase boundary.

tures and toughen the material, as in other biological or polymeric materials [2]. Previous studies on nanocomposites [2] have shown a minimal density of nanostructures is needed for toughening. In our experiments, the onset of toughening $\lambda_y = 3.8$ is beyond the onset of crystallization ($\lambda_y = 3$). This further supports the idea that the same toughening mechanism is at work in stretched natural rubber and other materials [2]. The idea of crystallization can also explain the phase separation in photo-elastic pictures. Upon sufficient relaxation, the crystallites melt and the material returns to the amorphous state [7].

Many microscopic mechanisms have been proposed to explain the toughening effect due to the interweaving of soft (amorphous) and hard (crystalline) substances at nanometer scales. Many authors [5] have proposed that soft regions can greatly weaken the stress concentration at the crack tip. Others [2] suggest that mechanical heterogeneity relieves the triaxial stress state and promote shear yielding of the polymer matrix, which forces polymers to slide against others, dissipating energy and toughening. While it seems likely that such theories will ultimately explain the toughening we have observed, our understanding of the details of crystallization in rubber is not yet sufficient to provide quantitative estimates.

To demonstrate the relation between crystallinity and toughness indirectly, we prepared a series of specimens with the same stretch ratio λ_y but of different heights h. The phase diagram, in the inset of Fig. 4, shows that for a given stretch ratio λ_y, there is a critical specimen height $h_c(\lambda_y)$ such that fractures can only propagate in specimen larger than $h_c(\lambda_y)$. This critical height increases rapidly as λ_y approaches 4.2. The elastic energy stored in the specimen of critical height $h_c(\lambda_y)$ also increases rapidly as a function of the stretch as shown in Fig. 4; the stored elastic energy is not indicative of fracture resistance in a conventional sense, but instead is associated with the energy consumed by a propagating structure surrounded by phase transformations of strain crystallizing material. Quantitative models of crystallization and its role in the elastic, viscous and fracture response of rubber remain to be developed.

Conclusions.—We have studied fracture propagation in natural rubber sheets stretched at different ratios λ_y. Two regimes with very different fracture resistance were found. For $\lambda_y < 3.8$, experimental results can be explained by a numerical model based on neo-Hookean theory and Kelvin dissipation. For $\lambda_y > 3.8$, significant strain-induced crystallization occurs throughout the prestretched specimen and greatly increases fracture resistance.

Our work suggests an alternative way to produce materials toughened by nanostructures. Instead of introducing external fillers into the matrix [1,3], we can produce *in situ* fillers through phase transitions induced by macroscale deformations in materials such as natural rubber, polybutadiene and butyl rubber [15]. This new method may be able to produce uniformly distributed fillers, which are hard to achieve in conventional methods.

[1] Y. C. Ahn and D. R. Paul, Polymer **47**, 2830 (2006).
[2] L. Corte and L. Leibler, Macromolecules **40**, 5606 (2007).
[3] T. X. Liu, I. Y. Phang, L. Shen, S. Y. Chow, and W. D. Zhang, Macromolecules **37**, 7214 (2004).
[4] J. M. Gosline, P. A. Guerette, C. S. Ortlepp, and K. N. Savage, J. Exp. Biol. **202**, 3295 (1999).
[5] K. Okumura and P. G. de Gennes, Eur. Phys. J. E **4**, 121 (2001); H. J. Gao, B. H. Ji, I. L. Jager, E. Arzt, and P. Fratzl, Proc. Natl. Acad. Sci. U.S.A. **100**, 5597 (2003).
[6] L. Treloar, *The Physics of Rubber Elasticity* (Oxford University Press, New York, 1975).
[7] S. Trabelsi, P. A. Albouy, and J. Rault, Macromolecules **36**, 7624 (2003).
[8] S. Poompradub, M. Tosaka, S. Kohjiya, Y. Ikeda, S. Toki, I. Sics, and B. S. Hsiao, J. Appl. Phys. **97**, 103529 (2005).
[9] P. J. Petersan, R. D. Deegan, M. Marder, and H. L. Swinney, Phys. Rev. Lett. **93**, 015504 (2004).
[10] G. J. Lake, C. C. Lawrence, and A. G. Thomas, Rubber Chem. Technol. **73**, 801 (2000).
[11] M. Marder, J. Mech. Phys. Solids **54**, 491 (2006).
[12] H. P. Zhang, J. Niemczura, G. Dennis, K. Ravi-Chandar, and M. Marder, Int. J. Fract. (to be published).
[13] K. B. Broberg, *Cracks and Fracture* (Academic Press, New York, 1999).
[14] G. J. Lake and A. G. Thomas, in *Engineering with Rubber*, edited by A. N. Gent (Hanser Publishers, Munich, 2001).
[15] S. Toki, B. S. Hsiao, S. Kohjiya, M. Tosaka, A. H. Tsou, and S. Datta, Rubber Chem. Technol. **79**, 460 (2006).